EXPERIMENTAL AND NUMERICAL STUDY OF THE MOISTURE DIFFUSION IN ADHESIVE COMPOSITE JOINTS

L. P. Canal[a*], R. Sarfaraz[b], G. Violakis[c], V. Michaud[a], J. Botsis[b], H. G. Limberger[c]

[a]*Laboratory for Polymer and Composite Technology (LTC).*
[b]*Laboratory of Applied Mechanics and Reliability Analysis(LMAF).*
[c]*School of Engineering.*
Ecole Polytechnique Fédérale de Lausanne (EPFL).CH-1015 Lausanne, Switzerland.
**luis.canal@epfl.ch*

Keywords: Adhesive joints, Smart materials, Strength, Fiber Bragg gratings, Finite element analysis (FEA)

Abstract
Water diffusion into adhesively bonded composites was experimentally studied by means of water intake measurements in bonded specimens as well as in the glue and in the composite alone. In addition, Fiber Bragg grating sensors were employed for the detection of absorbed water through the strain caused by swelling of the material. A finite element model was developed to simulate the water diffusion into the adhesive composite joint and the response of the optical sensor. Mass gain and strains versus time were in agreement with the experimental results.

1. Introduction

Adhesive bonding of composite structures is an adequate technique to assemble lightweight structures, which has been increasingly used in industries such as construction, automotive, sports, etc. However, in spite of the expected weight reductions, the use of adhesive composite bonds in aeronautical applications is limited by the possible deterioration of the joint upon exposure to environmental contaminants and the lack of adequate techniques to monitor the quality of the bond. Moisture contamination is probably the most studied scenario in polymers and composite materials [1-3], and numerous models have been proposed to describe this process [4-6]. Nevertheless, the diffusion of water in adhesive composite bonds is not well understood due to the heterogeneous microstructure of the composite and its interface with the adhesive layer [7, 8]. Furthermore, since the presence of moisture cannot be easily detected by conventional non-destructive tests, its negative effects are even more dangerous for the integrity of the composite structure.

The ideal adhesive joint configuration consists of two or more composite parts bonded together with a thin adhesive layer (0.1-0.3 mm thick), which transmits the loads mainly in shear, minimizing peel stresses [9]. In this geometry the surface of adhesive directly exposed to the environment is very small, but moisture can still diffuse through the composite adherents and contaminate the bond. The absorption of water produces swelling of the epoxy matrix in the composite parts and of the adhesive in the joint. Additionally, due to the presence of carbon fibers, the swelling properties are very anisotropic, resulting in multiaxial strain states, which can be monitored using fiber Bragg gratings (FBGs) embedded at appropriate locations in the bond. The present work aims at assessing the suitability of using

FBG sensors to detect the presence of moisture in adhesive composite joints from very early stages. The water diffusion properties of the components of the composite bonds were characterized by means of gravimetric methods. Simultaneously, their swelling coefficients were experimentally measured using embedded FBGs. The relevant material properties of the composite and the adhesive in dried and saturated states were determined through dynamic-mechanical analysis (DMA) test. This information was employed to simulate the swelling of the composite adhesive joint.

2. Materials and experimental techniques

2.1 Fiber Bragg grating sensor principles

A fiber Bragg grating sensor consists of a periodic change in the refractive index of the core of an optical fiber along a small segment. Thus, in a uniform grating, when white light is transmitted through an optical fiber containing a FBG, a narrow-band of light is reflected back. The wavelength of the light reflected by the Bragg grating, λ_B, depends on the effective refractive index of the fiber core, n_{eff}, and the grating period, Λ, [10]:

$$\lambda_B = 2n_{eff}\Lambda \tag{1}$$

The value of the reflected Bragg wavelength is sensitive to mechanical and thermal loads, producing a shift in the Bragg wavelength, $\Delta\lambda_B$, which can be related to the strains in the optical fiber as:

$$\frac{\Delta\lambda_{B,x}}{\lambda_{B,x}} = \varepsilon_z - \frac{n_{eff}^2}{2}\left[p_{11}\varepsilon_x + p_{12}\left(\varepsilon_y + \varepsilon_z\right)\right] + \left(\alpha_f + \xi_f\right)\Delta T \tag{2}$$

$$\frac{\Delta\lambda_{B,y}}{\lambda_{B,y}} = \varepsilon_z - \frac{n_{eff}^2}{2}\left[p_{11}\varepsilon_y + p_{12}\left(\varepsilon_x + \varepsilon_z\right)\right] + \left(\alpha_f + \xi_f\right)\Delta T \tag{3}$$

where ε_z is the axial strain on the fiber and $\varepsilon_x, \varepsilon_y$ are the two lateral ones, ; p_{11} and p_{12} are the Pockel's strain-optic coefficients ; α_f is the thermal expansion ; ξ_f the thermo-optic coefficient of the optical fiber ; ΔT the change in temperature.

A change in temperature ΔT or water uptake $\Delta wt\%$ leads to longitudinal and transversal strains, i.e. $\varepsilon_i = f\left(\Delta T, \Delta wt\%\right)$, where i stands for x,y or z. When the longitudinal strain is the dominant component in an axi-symmetric configuration, the transversal strains are linked to the longitudinal strain using Poisson's ratio, $\varepsilon_x = \varepsilon_y = -\nu\varepsilon_z$ which leads to

$$\frac{\Delta\lambda_B}{\lambda_B} = \left(1 - p_e\right)\varepsilon_z + \left(\alpha_f + \xi_f\right)\Delta T \tag{4}$$

where the effective photoelastic coefficient is given by $p_e = \frac{1}{2}n_0^2\left[p_{12} - \nu\left(p_{11} + p_{12}\right)\right]$. For silica p_e=0.22.

The optical fibers employed in this study were standard single mode SMF-28 fibers with polyamide coating. The FBGs were fabricated in these fibers using the phase mask technique and an ArF excimer laser. The phase mask pitch Λ_{pm} was 1060 nm and the typical irradiation conditions were a fluence per pulse of ~100 mJ/cm^2, 10 Hz repetition rate and ~20 minutes total irradiation time. The resulting FBGs had a length of 10 mm and typical reflectivity of 60-70%. Water uptake experiments were conducted at constant temperature, i.e. $\Delta T = 0$.¨

2.2 Materials and specimens

The composite panels were prepared from unidirectional prepregs of M21/T700. The prepreg sheets were stacked in the sequence $[0, 90]_s$ and consolidated in the autoclave under 7 bar pressure and 180 °C during two hours. The adhesive layer was Cytec FM-300 K 0.5. This is a modified epoxy adhesive with a wide open knit polyester carrier. The diffusion of water into adhesive composite joints was investigated in specimens made from two cross-ply composite panels bonded together with the epoxy film adhesive. The adhesive was heated at 3 °C /min and consolidated at 175 °C in the autoclave under 3 bar pressure for 60 minutes. Before achieving the curing temperature, a vacuum outgassing step at 110 °C for 30 minutes was applied to minimize the porosity of the specimen. Four bond specimens were prepared by joining together two CFRP square parts with one ply of adhesive; the final dimensions of these specimens were ≈100x100x1.96 mm^3. Two of the bond specimens were employed to study the water diffusion through gravimetric methods. In two other specimens, an optical fiber with one FBG was embedded in the glue ply prior to processing (Fig. 1).

Figure 1. a) Schematic of the composite bond structure: optical fiber placed in the middle of a glue layer and between two cross-ply CFRP plates **b)** Micrograph of the optical sensor placed in the bond specimen.

CFRP and bulk adhesive specimens were also prepared to characterize the mechanical and diffusion properties of the bond components. Several plies of the adhesive film were stacked and consolidated in the autoclave to manufacture square bulk adhesive specimens for water absorption. Differential scanning calorimetry (DSC) analysis was carried out using a DSC TA Q100 under the form of heating ramps from 20 to 250 °C at 10 °C /min to confirm that the adhesive was fully cured after this curing cycle. The final dimensions of the specimens were ≈130x130x1.25 mm^3. The swelling of the adhesive upon the absorption of water was characterized in one additional specimen with one embedded optical fiber (Fig. 2a). Water absorption experiments were also conducted on two unidirectional and two bidirectional specimens of M21/T700 CFRP with dimensions according to the recommendations of the ASTM standard for the determination of the absorption properties in composite materials [11]. These specimens were manufactured by stacking four plies of M21/T700 prepreg and consolidated in the autoclave. The final dimensions of the specimens were ≈100x100x0.88 mm^3. The swelling of the CFRP upon the absorption of water was characterized by unidirectional specimens of M21/T700 CFRP carbon fiber reinforced polymer (CFRP) with optical fibers integrated along and perpendicular to the carbon fibers, respectively (Fig. 2b, c)

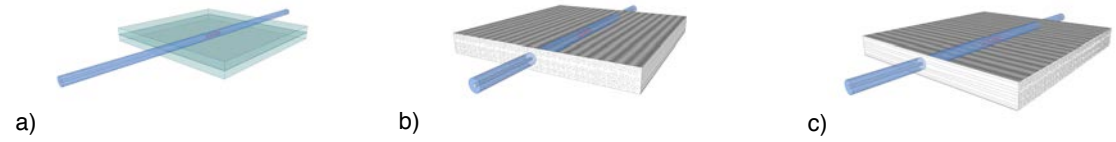

Figure 2: Schematic of the samples: Bulk adhesive (a), CFRP with FBG parallel (b) and perpendicular (c) to the carbon fibers.

All the specimens, bulk or bonded joints, were dried in an oven at 70 °C during two weeks, weighted and immersed in demineralized water at 70 °C. The mass gain of the specimens for gravimetric measurements was periodically monitored using a scale with a precision of 0.1 mg. The spectrum of the samples with FBGs was monitored at a fixed time interval (24 h) using an FBG interrogator (MicronOptics SM125) with a resolution of 5 pm. The wavelength shift was extracted from the spectral data. Mechanical properties of the adhesive and the composite in dry and water-saturated states were studied with a dynamic mechanical analyzer (DMA Q800, TA Instruments, USA). The DMA samples were rectangular with approximate dimensions 15 x 6 x 1 mm^3. The tests were carried out in tension mode with a sinusoidal strain of 0.01% at 1 Hz and a temperature ramp of 5 °C /min between ambient and 180 °C.

3. Experimental results

3.1 Water absorption and swelling properties of the bulk constituents

The mass gained in the bulk adhesive specimens during their immersion in water at 70 °C is plotted in Fig. 3. The experimental data show very fast increment in the weight during the initial 250 hours, reaching a saturation of $s \approx 3.1$ wt%. Fick's law describes the mass gained during the initial 220 hours, using a diffusivity parameter of $D_{FM300} = (1.26 \pm 0.08) \times 10^{-6}$ mm^2/s. However, this model predicted an unrealistic and fast saturation, lower than the value experimentally obtained. This deviation from Fick's law in the mass gained in specimens of FM-300 adhesive is in agreement with the observations of LaPlante et al. [6], and is taken into account by including time-dependent boundary conditions [8]. Figure 3b shows the Bragg wavelength shift during water uptake. A positive single wavelength shift of up to 7 nm within the first 220 h was observed. After a slight decrease the signal stabilized at about 6.5 nm. In this sample the wavelength shift is due to a longitudinal fiber strain with equal transversal strains. The swelling coefficient, defined by the maximum strain obtained at 220h was calculated from Eq. 4 with ($\Delta T=0$, s=3.1 wt%, $\Delta\lambda_{B,\max} / \lambda_B = 4.6 \times 10^{-3}$) as $\beta = \frac{1}{s}\frac{1}{(1-p_e)}\frac{\Delta\lambda_{B,\max}}{\lambda_B}$. A value of $\beta_{FM300} = (1900 \pm 200)$ με/wt% was obtained.

Water uptake in uni and bidirectional M21/T700 CFRP specimens was periodically monitored during immersion in distilled water at 70 °C (Fig 4a). The experimental measurements showed a faster mass gain for the bidirectional specimens. The experimental data for both configurations could be fitted using Fick's diffusion law. The diffusivity and saturation parameters obtained were $D_{CFRP\_unidir} = (1.2 \pm 0.2) \times 10^{-7}$ mm^2/s, $D_{CFRP\_bidir} = (2.5 \pm 0.3) \times 10^{-7}$ mm^2/s, $s_{CFRP\_uni} = (1.3 \pm 0.1)$ wt% and $s_{CFRP\_bidir} = (1.3 \pm 0.2)$ wt%. Figure 4b shows the FBG wavelength shift due to swelling of the CFRP in the directions parallel and perpendicular to the reinforcement carbon fibers during water uptake in unidirectional specimens.

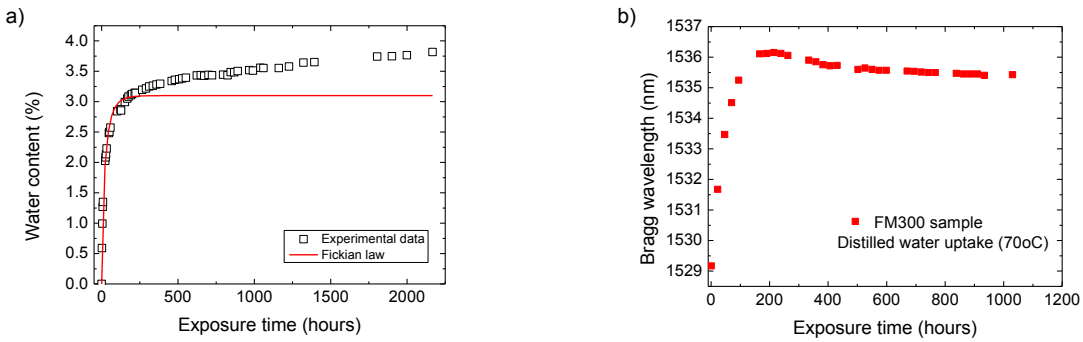

Figure 3. Water absorption **a**) and evolution of the Bragg wavelength. Shift **b**) in the adhesive specimen FM-300K (immersed in water) as a function of time at 70 °C.

The FBG sensor placed along the direction of the carbon fibers did not measure any noticeable strain variation during the water absorption, but the FBG in the optical fiber oriented perpendicular to the reinforcement showed an important positive wavelength shift of up to 6 nm. The strain increase is due to the swelling of the laminate in the direction perpendicular to the carbon fibers. The swelling coefficient of the material in this direction was obtained from the maximum strain measured at saturation using Eq. 4 ($\Delta T=0$ and $s=1.3$, $\Delta\lambda_{B,\max} / \lambda_B = 3.95 \times 10^{-3}$): $\beta_{\perp CFR} = 3900 \pm 200$ με/%.

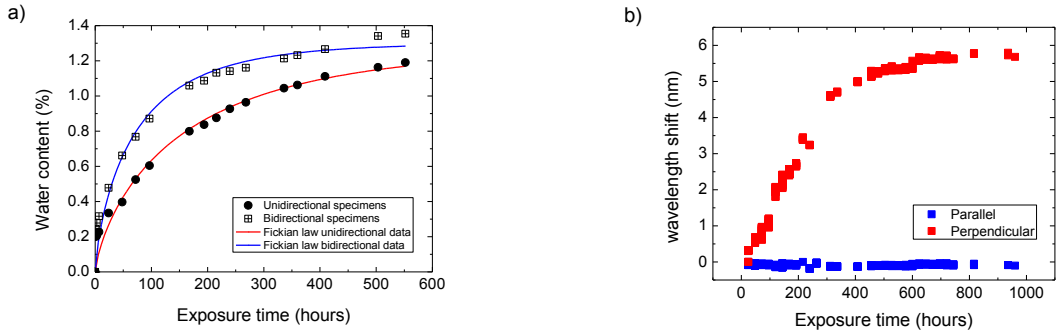

Figure 4. a) Water absorption plot from M21/T700 specimens in water at 70 °C. **b)** FBG wavelength evolution in the composite plates immersed in water as a function of time.

3.2 Mechanical properties of the bulk constituents in dry and saturated state

Absorption of water by the epoxy produces a noticeable reduction in the elastic properties of the adhesive and the epoxy-matrix composites. Thus, realistic simulations of the strains detected by the optical sensors embedded in the specimens during water uptake should rely on accurate material properties for the adhesive and composite in the studied conditions. For this reason, DMA tests were carried out in dry and saturated specimens of FM 300K and M21/T700 CFRP. Storage modulus in the adhesive and perpendicular to the reinforcement in the CFRP are plotted in Fig. 5, as a function of temperature. In both cases the saturated specimens showed a reduction of the elastic modulus compared to the dried state. Furthermore, T_g decreased by ≈ 10°C, as previously reported [12].

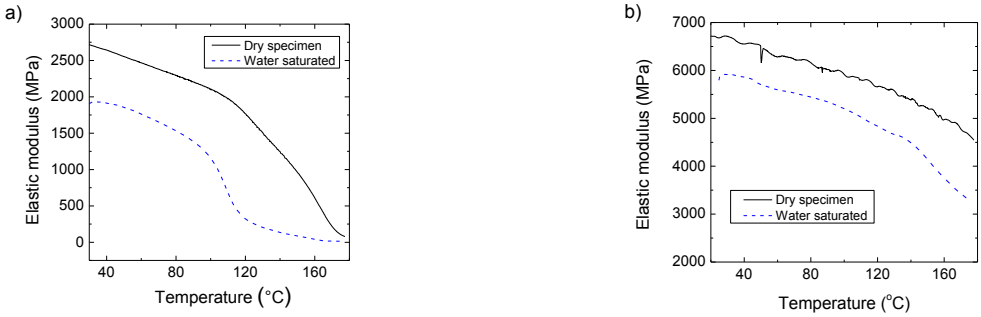

Figure 5. Temperature evolution of the storage modulus of a) the adhesive and b) the CFRP in perpendicular direction to the reinforcement for dry and water-saturated specimens..

3.3 Water uptake in the bond specimen

The mass gained in the bond specimens is plotted in Fig. 6a. The shift in the reflected spectrum of the FBG embedded in the joint specimens is shown in Fig. 6b. Two peaks are observed, as a result of the birefringence induced by the residual strains developed after the consolidation and cool down of the adhesive during the bond manufacturing. Swelling due to the absorption of water in the joint led to a shift of these two peaks (Fig. 6b). Both peaks had a different sensitivity to swelling. Peak 2 was almost stabilized after ≈250 hours for a shift of ≈ 0.22 nm whilst peak 1 continued to evolve until a maximum shift of 0.38 nm after 1200

hours. The difference in the maximum shift of Bragg peak 2 of the two samples is due to sample to sample variation of the manufacturing induced initial birefringence.

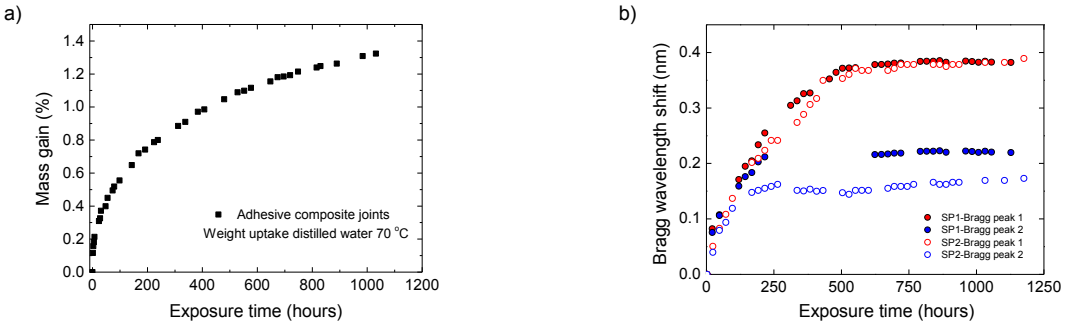

Figure 6. a) Water absorption plot joint specimens in water at 70 °C. **b)** Evolution of the Bragg peak due to water uptake of the composite laminate at 70°C.

4. Computational models

Water diffusion in adhesive joints is a complex mechanism, which depends on the microstructures involved. Accurate simulations of this process require numerical microscale models [8], which cannot be easily applied due to their high computational cost. Thus, water absorption and swelling of the bond specimen was simulated through a 3D model of one eighth of the sample in which CFRP and glue were considered as homogeneous materials. The presence of the optical fiber was explicitly taken into account in the geometry. The CFRP was simulated as an anisotropic homogeneous material, with diffusion properties obtained from the water uptake experiments in bidirectional CFRP specimens. The water uptake measurements in the FM-300K specimens were also employed to obtain the diffusion properties for the adhesive layer. The diffusivity through the thickness of the joint was approximated by the diffusivity of the cross ply composite part. The analogy between heat and mass transfer was employed to simulate the water uptake experiment through a coupled temperature-displacement model in Abaqus [13]. The Young's moduli of the adhesive at 70 °C, in dry and saturate states, were obtained from the DMA measurements (Fig. 5a). The same experimental technique was employed to find the Young's modulus of CFRP in the direction perpendicular to the reinforcement (Fig. 5b). The other elastic constants necessary to describe the mechanical behavior of the anisotropic material were obtained from the Mori-Tanaka homogenization model (Table 1).

	Diffusivity (mm^2/s)			**Saturation (%)**
	D_{11}	**D_{22}**	**D_{33}**	
CFRP	$(1 \pm 0.1)\times 10\text{-}7$	$(1 \pm 0.1)\times 10^{-7}$	$(2.5 \pm 0.3)\times 10^{-7}$	1.3
Adhesive	$(12.6 \pm 0.1)\times 10\text{-}7$	$(12.6 \pm 0.1)\times 10\text{-}7$	$(12.6 \pm 0.1)\times 10\text{-}7$	4

Table 1. Diffusion properties of the CFRP and the adhesive employed in the simulations.

	Young's modulus (GPa)		**Shear modulus (GPa)**		**Poisson's ratio**	
	E_{11}	**$E_{22}= E_{33}$**	**$G_{12}=G_{13}$**	**G_{23}**	**$\nu_{12}=\nu_{13}$**	**ν_2**
CFRP (dry70 °C)	139	6.2	6	4.1	0.25	0.4
CFRP (saturated70 °C)	139	5.5	5.5	3.8	0.25	0.4
Adhesive (dry70 °C)	2.38				0.4	
Adhesive (saturated70 °C)	1.7				0.4	
Optical fiber	70				0.16	

Table 2. Elastic properties of the CFRP, adhesive and optical fiber employed in the simulations.

5. Simulation results and discussion

The numerical prediction of the mass gained in the bond specimen during immersion in water at 70 °C is plotted in Fig. 7a together with the experimental results. Finite element simulations were able to reproduce the diffusion kinetics experimentally measured. The numerical model of the joints was also applied to the evolution of strains on the optical fiber during the water absorption test. Thus, the shift of the reflected Bragg peaks was computed through equations 2 and 3, and plotted in Fig. 7b. The two peaks appear, and have a different water swelling response. The initial behavior of both peaks followed the experimental data well. Peak 2 almost stabilized for a shift of ≈0.2 nm after 500 hours, while peak 1 is in good agreement with the experimental data up to 750 h.

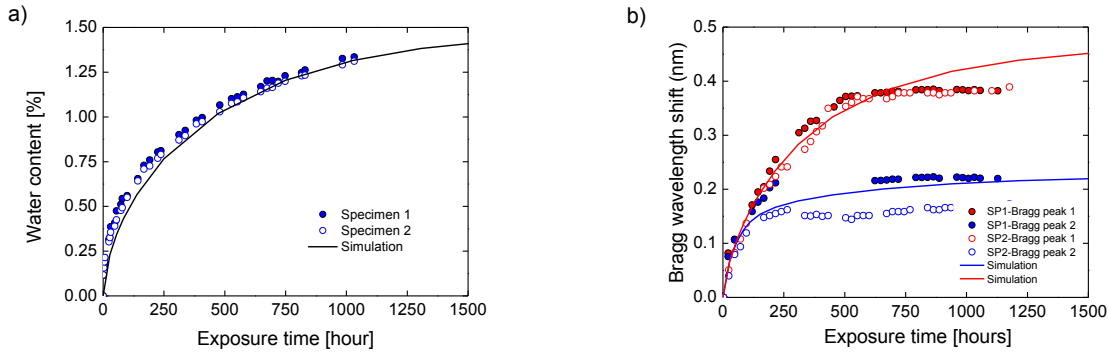

Figure 7. Numerical and experimental results of **a)** the mass gained and **b)** Bragg peak evolution due to water uptake of the composite laminate at 70°C.

The simulated swelling sensitivity of the Bragg peaks showed a good agreement with the experimental results (Fig. 8). The optical sensor has a small response for water absorbed below 0.2%, and a high sensitivity to water content between 0.2 and 1.2 %. In this range peak 1 showed an almost linear response, which also depends on the geometry of the specimen.

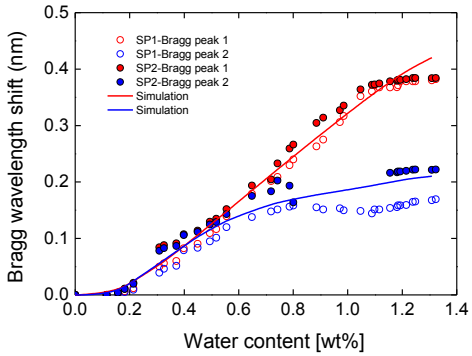

Figure 8. Swelling sensitivity of the Bragg peaks.

6. Conclusions

The water diffusion into composite adhesive joints was experimentally studied by means of gravimetric measurements in bond specimens. The main parameters controlling the diffusion in the bond components were obtained, following the standard processes, from water-uptake experiments carried out in specimens of fiber-reinforced composite and epoxy adhesive. Numerical simulations were able to accurately predict the mass gained due to the water uptake and the mechanisms of diffusion through the composite microstructure. The

coefficients of moisture expansion in these materials were also obtained by embedding FBG sensors in the specimens. The adhesive composite joints with FBG integrated into the glue layer showed a maximum shift of 0.38 nm due to water uptake at 70 °C after 1200 hours. Additionally, and simulations were able to reproduce these measurements. According to these results, water concentrations as low as 4‰ can be detected.

Acknowledgements
The research leading to these results has received funding from the European Union Seventh Framework Programme (FP7/2007- 2013) under Grant Agreement No. 266226 (ENCOMB, Extended Non-Destructive Testing of Composite Bonds).

References

[1] G. Pogany, Anomalous diffusion of water in glassy polymers, Polymer 17 (1976) 690-694.
[2] A. Apicella, R. Tessieri, C. de Cataldis, Sorption modes of water in glassy epoxies, Journal of Membrane Science 18 (1984) 211-225.
[3] R. Selzer, K. Friedrich, Mechanical properties and failure behaviour of carbon fibre-reinforced polymer composites under the influence of moisture, Composites part A 28 (1997) 595-604.
[4] H. G. Carter, K. G. Kibler, Langmuir-type model for anomalous moisture diffusion in composite resins, Journal of Composite Materials 12 (1978) 118-131.
[5] Y. Weitsman, A continuum diffusion model for viscoelastic materials, The Journal of Physical Chemistry 94 (1990) 961-968.
[6] G. LaPlante, P. Lee-Sullivan, Moisture effects on fm300 structural film adhesive: stress relaxation, fracture toughness and dynamic mechanical analysis, Journal of Applied Polymer Science 95 (2005) 1285-1294.
[7] S. J. John, A. J. Kinloch, F. L. Matthews, Measuring and predicting the durability of bonded carbon fibre/epoxy composite joints, Composites 22 (1991) 121-127.
[8] L. P. Canal, V. Michaud, Micro-scale modeling of water diffusion in adhesive composite joints, Composite Structures (in press).
[9] L. F. M. da Silva, R. D. Adams, Techniques to reduce the peel stresses in adhesive joints with composites, International Journal of Adhesion and Adhesives 27 (2007) 227-235.
[10] K. O. Hill, G. Meltz, Fiber bragg grating technology fundamentals and overview, Journal of Lightwave Technology 15 (1997) 1263-1273.
[11] D5229, Standard Test Method for Moisture Absorption Properties and Equilibrium Conditioning of Polymer Matrix Composite Materials, ASTM International, West Conshohocken, PA, 2012.
[12] M. Lai, J. Botsis,J. Cugnoni, D. Coric, An experimental–numerical study of moisture absorption in an epoxy, Composites Part A: Applied Science and Manufacturing 43 (2012) 1053–1060.
[13] Abaqus, Users' Manual, version 6.12, ABAQUS, Inc. 2012.
[14] T. Mori, K. Tanaka, Average stress in matrix and average elastic energy of materials with misfitting inclusions, Acta Metallurgica 21, (1973), 571-574.